Microscopic theory of impurity states in coupled quantum wells and superlattices

D. Stehr and M. Helm
Institute of Ion Beam Physics and Materials Research, Forschungszentrum Rossendorf, P.O. Box 510119, D-01314 Dresden, Germany

C. Metzner
Biophysics Group, Center for Medical Physics and Technology, University of Erlangen, D-91052 Erlangen, Germany

M. C. Wanke
Sandia National Laboratories, P.O. Box 5800, Albuquerque, New Mexico 87185, USA
(Received 19 April 2006; revised manuscript received 17 May 2006; published 18 August 2006)

We present a theory of impurity states in quantum wells and superlattices which treats the confining heterostructure potential and the random impurity potential on the same footing. The relevant three-dimensional Hamiltonian is diagonalized in the low-doping regime. The results are used to calculate infrared absorption spectra which contain contributions of impurity and intersubband transitions. We mainly discuss the excited impurity states, which are pinned to higher subbands and are resonant states in the continuum. After a detailed analysis of a coupled quantum well system, we study the transition to a superlattice. In particular, we are able to explain existing experimental data on a quadruple quantum well.

DOI: 10.1103/PhysRevB.74.085311 PACS number(s): 73.20.Hb, 73.21.Cd, 73.21.Fg, 78.67.De

I. INTRODUCTION

Semiconductor heterostructures represent the basis for many (opto)electronic devices, such as lasers or detectors. Yet they can also play a role as model systems for fundamental processes in solid-state physics, since quantum wells (QWs) or superlattices (SLs) of very high structural and electronic quality can be fabricated. Semiconductor superlattices, for instance, have provided the first example for the experimental demonstration of Bloch oscillations.[1]

For many applications structures doped with electrons are required. Important examples are "band-structure engineered" infrared devices making use of intersubband transitions such as quantum cascade lasers (QCLs) or quantum well infrared photodetectors (QWIPs).[2] Consequently the properties of shallow impurity levels in quantum wells and superlattices have first been studied 25 years ago,[3,4] and some detailed understanding has been achieved.[5,6] Most theoretical work has been concerned with variational approaches, considering only selected, and often low-lying impurity states. In this work we present a calculation of the energy levels of the combined quantum well and random-impurity system, where quantum well potential and impurity potential are treated on the same footing. We will show that this approach leads to considerable insight and unveils some interesting features. In order to facilitate comparison with experimental data, we use the results to calculate infrared absorption spectra, exhibiting intersubband and impurity transitions according to the thermal occupation of the respective energy levels. The nature of the states—impuritylike or bandlike—is analyzed by looking at the wave functions in the planes of the confined layers.

The present paper is organized as follows. First (Sec. II) we give a brief account of the most important properties of shallow impurity levels in quantum wells and superlattices. In Sec. III we present our theoretical method of calculating the energy levels and the resulting infrared absorption spectra. Section IV is devoted to a detailed discussion of a symmetric double-quantum well system, which is still relatively simple, but leads to some significant physical insight. In section V the properties of a quadruple quantum well structure will be elaborated. Here we present old, but unpublished, experimental data, which can be explained with our calculation to a very high degree of perfection. In addition we will discuss the transition from a finite system to a superlattice, modeled by considering 20 coupled quantum wells. Finally the paper is concluded with a summary and an outlook.

II. BASIC PROPERTIES OF CONFINED IMPURITY STATES

In a bulk semiconductor the energy levels of shallow donors can be well described in the usual scheme for hydrogen atoms with the quantum numbers N, l (angular momentum), m (magnetic quantum number), i.e., the $1s$, $2s$, $2p$ ($m=\pm1,0$), $3s$, $3p$ ($m=\pm1,0$), $3d$ ($m=\pm2,\pm1,0$), etc., states with ground-state binding energy of one effective Rydberg, Ry^*. In two dimensions, the binding energy is four times higher, and also the level classification is different, e.g., the $2p$ state is only twofold degenerate. The exact two-dimensional limit corresponds to a situation with a single subband, and is only of limited relevance for realistic QWs. In a quasi-two-dimensional (2D) system with several subbands it is still possible and useful to employ the 3D classification, which, however, becomes modified by the QW potential. The breaking of the translation symmetry in the growth (z) direction removes the degeneracy of some states,[7] which become pinned to higher QW subbands.[8] Detailed analysis shows that states with low $|m|$ quantum numbers, which are the ones with largest extension in the z direction, are pushed up farthest, in particular the states $1s$ and $2p_{\pm1}$ are associated with the ground ($n=1$) subband, the states $2p_0$, $3d_{\pm1}$, etc., with the $n=2$ subband, the states $3d_0$, $4f_{\pm1}$ with the $n=3$ subband etc. The relation expressing the exact assignment of an impurity state (N,l,m) to a subband n reads

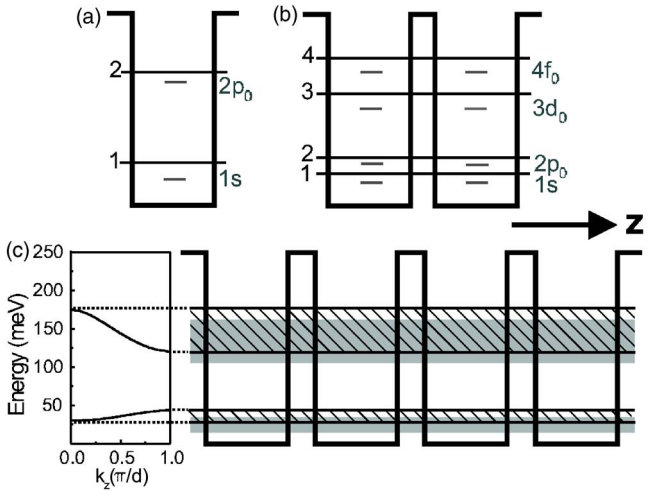

FIG. 1. Sketch of the subband levels and most important impurity levels (grey) for a single (a) and double (b) quantum well. In (c) the minibands (hatched) and impurity bands (grey shaded) for a superlattice are shown.

$n=l-|m|+1$.[9] The "most important" states are the $m=0$ states $(1s,2p_0,3d_0,\ldots)$ having z symmetry (except of course the $1s$), which become the ground states of a two-dimensional hydrogenic series attached to each subband. This is illustrated for a single quantum well in Fig. 1(a). It should be pointed out again that this labeling of the quasi-2D states with the 3D atomic notation is mainly a matter of convenience, but can be justified with the one-to-one correspondence.[9] The optical transition between the attached impurity ground levels $(1s-2p_0)$, follows the same selection rule as the usual intersubband transition, i.e., the exciting light needs to have an electric-field component parallel to the growth axis z. Due to the slightly larger binding energy of the $1s$ state with respect to the $n=1$ subband, as compared to the $2p_0$ state with respect to the $n=2$ subband, the $1s-2p_0$ transition occurs at a slightly higher photon energy than the $1\rightarrow 2$ intersubband transition, and can thus be regarded as an "impurity-shifted" intersubband transition. It is easier to observe in wide QWs, where the relative shift (relative to the intersubband energy) is larger;[10] in narrower quantum wells (<10 nm) it has only been observed recently.[11] Helm *et al.*[12] have shown that in strongly coupled superlattices the $1s-2p_0$ transition can be observed very clearly, since it is spectrally well separated from the van Hove singularities of the interminiband absorption spectra due to the finite miniband width. Yet recently we have shown that this needs a re-interpretation, since in fact in superlattices the $2p_0$ states form an excited impurity band, resonant with the excited miniband.[13] In this connection it is interesting to observe how an isolated quantum well evolves into a superlattice, consisting of many coupled quantum wells. This is best studied by looking at a coupled double quantum well system, which can, on the one hand, be analyzed as one quantum-mechanical entity with twice as many subbands as a single QW, but can also be regarded as a precursor to a superlattice. In this latter case the lower-state doublet $(n=1,2)$ evolves into the first miniband and the upper-state doublet $(n=3,4)$ into the second miniband [see Figs. 1(b) and 1(c)]. The $1\rightarrow 4$ and $2\rightarrow 3$ transitions in the coupled QW would thus correspond to the superlattice transitions at the mini-Brillouin center $(k_z=0)$ and edge $(k_z=\pi/d)$, respectively. The terminology for the impurity states, however, then acquires some ambiguity: Looking from the "one entity" perspective,[14] the main impurity states associated with the $n=1\ldots 4$ subband would be $1s$, $2p_0$, $3d_0$, $4f_0$, respectively [see Fig. 1(b)]. From the SL perspective, on the other hand, the $3d_0$ (and $4f_0$) state would rather be called a $2p_0$ state (or band). We will show below that the $1s-3d_0$ transition, which is dipole forbidden in a single quantum well, is actually allowed in a (strongly coupled) double QW, in contrast to the corresponding $1\rightarrow 3$ intersubband transition, a fact understandable from the SL perspective.

Therefore, in the following, we will discuss in detail the energy levels and absorption spectra of a double quantum well for different thicknesses of the coupling barrier. We will also study the influence of the doping density and impurity location in the QW plane. The double quantum well provides the advantage of relative simplicity and reasonably short computation time, but unfortunately there are no experimental data available on double QWs in the low- or intermediate-doping regime. Therefore we extend our calculation to quadruple quantum wells, where experimental absorption spectra are available and can be perfectly reproduced with our theory. Finally we sequentially increase the number of quantum wells and show how the typical QW absorption spectra evolve into superlattice absorption spectra, corroborating our recently published results on excited, resonant impurity bands.[13] For all calculated spectra, impurity transitions and subband transitions are observed, depending on doping and temperature, and are identified by looking at the wave functions of the energy levels involved.

III. METHOD OF CALCULATION

Previous calculations of impurity levels in quantum wells were often based on variational approaches,[3–5,7,15,16] which usually require some *a priori* assumptions concerning the impurity states. Also mostly low-lying levels have been investigated in the past. Yet already in 1984 Priester *et al.*[15] had shown that each 2D subband has an impurity band associated with it. Ghazali *et al.*[17] performed calculations of the density of states (DOS) in a multiple-scattering approach, and obtained also excited impurity levels,[18] however, they did not extend their calculation to continuum states. Kortus and Monecke[19] demonstrated the evolution of impurity states into 2D subbands in δ-doped layers without an external confining potential, while Hofmann *et al.*[20] calculated the DOS in a 2D system with random impurities and investigated the Coulomb gap. Recent calculations investigated a double QW, but only near the lowest subband doublet,[14] or reported an analytical approach for resonant impurity states in QWs.[21]

Here we treat quantum well and impurity potentials in a unified framework and follow the method introduced in Ref. 22. Our goal is to solve the 3D Schrödinger equation for the single-particle quantum states:

$$\hat{H}(x,y,z)\Psi^{(i)}(x,y,z)=E^{(i)}\Psi^{(i)}(x,y,z). \tag{1}$$

The Hamiltonian can be decomposed into a purely z-dependent part $\hat{H}_0$ and a "perturbation" $\Delta\hat{H}$:

$$\hat{H}(x,y,z) = \hat{H}_0(z) + \Delta\hat{H}(x,y,z). \tag{2}$$

The z part determines the 1D states of the undoped multiple quantum well system,

$$\hat{H}_0(z) = \frac{p_z^2}{2m} + V^{(qw)}(z), \tag{3}$$

while the perturbation contains the lateral kinetic energy and the random 3D Coulomb potential of the impurities:

$$\Delta\hat{H}(x,y,z) = \frac{p_{xy}^2}{2m} + V^{(imp)}(x,y,z). \tag{4}$$

We first compute the 1D subband states of the undoped system:

$$\hat{H}_0(z) f_n(z) = \epsilon_n f_n(z). \tag{5}$$

As solutions of a Schrödinger equation, the subband wave functions $f_n(z)$ form a complete, orthonormal set. Since they already incorporate the strong potential $V^{(qw)}(z)$ of the multiquantum well system, this set is especially well suited for expanding perturbed states of the system with respect to the z coordinate.

In order to treat the x-y directions, we assume an artificial lateral periodicity of the impurity arrangement. Ideally, the linear dimension of the unit cell (in our case 100 nm) is chosen much larger than the average distance between nearest-neighbor impurities. This allows us the use of plane waves as lateral basis functions. Thus the complete expansion of our 3D wave functions reads

$$\Psi^{(i)}(x,y,z) = \sum_{k_x k_y n} G^{(i)}_{k_x k_y n} e^{ik_x x} e^{ik_y y} f_n(z). \tag{6}$$

Inserting Eq. (6) into Eq. (1) transforms the continuum Schrödinger equation into a discrete matrix eigenvalue problem:

$$\sum_{k_x' k_y' n'} H_{k_x k_y n, k_x' k_y' n'} G^{(i)}_{k_x' k_y' n'} = E^{(i)} G^{(i)}_{k_x k_y n}. \tag{7}$$

For its numerical solution, the fundamentally infinite number of basis states is truncated to a tractable number of order 1000. The Hamilton matrix to be diagonalized is given by

$$H_{k_x k_y n, k_x' k_y' n'} = \delta_{k_x k_y n, k_x' k_y' n'} \left(\epsilon_n + \frac{\hbar^2 (k_x^2 + k_y^2)}{2m} \right) + \langle k_x k_y n | V^{(imp)} | k_x' k_y' n' \rangle. \tag{8}$$

In principle, the optical transition between two quantum states (i) and (j) can directly be computed from the resulting coefficients $G^{(i)}_{k_x k_y n}$ and $G^{(j)}_{k_x k_y n}$, respectively. However, it is often instructive to back-transform the states into real-space representation. For this purpose, we first introduce the definition of lateral wave functions $g_n^{(i)}(x,y)$ attached to the different subbands n:

$$g_n^{(i)}(x,y) = \sum_{k_x k_y} G^{(i)}_{k_x k_y n} e^{ik_x x} e^{ik_y y}. \tag{9}$$

We can then write the expansion Eq. (6) in the more intuitive form

$$\Psi^{(i)}(x,y,z) = \sum_n f_n(z) g_n^{(i)}(x,y). \tag{10}$$

This expression shows the possibility of subband mixing arising from the (impurity-related) 2D lateral functions $g_n^{(i)}(x,y)$, which is of crucial importance in the case of energetically close subbands like in coupled quantum wells and superlattices. In the case of a narrow single quantum well, where the subbands are largely separated in energy, this can be neglected.[23] Note that this method, namely the exact solution of the complete 3D system and treatment of impurity potential and QW potential on the same footing, differs significantly from variational methods, which have been the main tool to describe impurity states especially in confined systems in the past, and where certain preassumptions have to be made beforehand.

With the resulting wave functions $\Psi^{(i)}(x,y,z)$ (several hundreds for a double QW or up to thousands for a SL) we then proceed in calculating the absorption coefficient α for light polarized in the z direction via Fermi's "golden rule" in dipole approximation:

$$\alpha(\hbar\omega) \propto \sum_{i,f} |\langle \Psi_f | p_z | \Psi_i \rangle|^2 (F_i - F_f) \delta(E_f - E_i - \hbar\omega). \tag{11}$$

Here F_i and F_f are the Fermi-Dirac occupation probabilities of the initial and final state. In order to remove artifacts due to one specific impurity configuration, and to obtain data directly comparable to real absorption measurements, we finally average this result over several (up to ten) additional random impurity configurations. The absorption spectra are obtained by using a Lorenztian line shape for each transition with a phenomenological broadening parameter Γ, representing the half width at half maximum.

IV. RESULTS FOR THE DOUBLE QUANTUM WELL

In this part we discuss the calculated absorption spectra of a lightly doped (few 10^{10} cm^{-2}) coupled GaAs/$Al_xGa_{1-x}As$ double QW (d_{well}=9.0 nm, d_{barr}=2.5 nm) in the mid-infrared (MIR) and far-infrared (FIR) regions. We will also vary the thickness of the coupling barrier and the electron density, and show the effects of directly placed dopants.

Figure 2 shows the absorption spectra calculated for different lattice temperatures and a phenomenological broadening of Γ=4 meV. The doping was set to 1×10^{10} cm^{-2} per QW, corresponding to one impurity in a 100×100-nm^2 area, and put in the center of each QW in the z direction. It was checked that at 4 K the Fermi energy is below the lowest extended (subband) state, this implies that all transitions observed at 4 K are due to impurity transitions. Shown are the FIR region (<20 meV), dominated by transitions to states near the first subband doublet of the double QW, and the

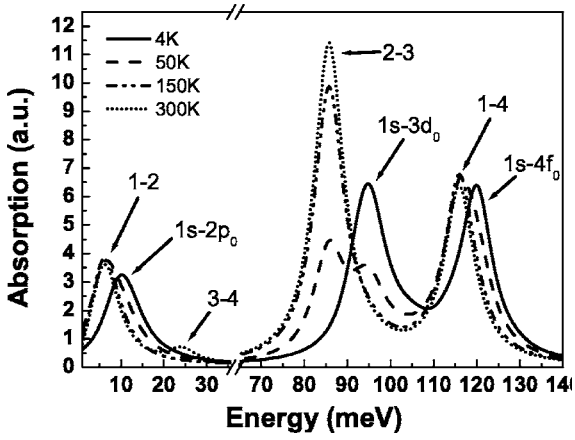

FIG. 2. Calculated absorption of a double quantum well for different temperatures.

MIR region (here 70–140 meV), dominated by transitions to states near the second doublet. Let us first analyze the spectrum at $T=4$ K. It consists of three peaks, one in the FIR and two in MIR. As we have shown before,[13] both MIR peaks can be attributed to transitions between localized states, one at 95 meV to the $1s$-$3d_0$ and one at 120 meV to the $1s$-$4f_0$ transition. Both final states have slightly lower energy than their corresponding subband states 3 and 4.

Upon increasing the lattice temperature, we observe drastic changes in the spectrum:

(i) The high-energy peak at 120 meV slightly shifts towards lower energy (116 meV). This is due to decreasing localization of the corresponding wave functions, leading finally to a pure intersubband transition $1\rightarrow 4$.[13]

(ii) The peak at 95 meV disappears rapidly with rising temperature and an additional peak at 85 meV becomes dominant. This is due to thermal occupation of the second subband, leading to absorption into the third subband.

(iii) Also the low-energy peak gets redshifted, again reflecting the transition from impurity states to extended (subband) states with rising temperature. The peak at 6 meV denotes the $1\rightarrow 2$ transition.

(iv) Finally, at $T=300$ K another peak shows up at 24 meV; at this high temperature, even the third subband becomes slightly occupied resulting in the transition into the fourth subband.

TABLE I. List of strongest transitions at $T=4$ K (left) and $T=300$ K (right). Listed are the initial (i) and final (j) states of each transition, their respective oscillator strengths f_{ij} and energies ϵ_{ij}. The transition in the third line at $T=300$ K is the strongest around 116 meV, but only the 23rd overall. The wave functions of the bold states are plotted in Figs. 3 and 4.

4 K			300 K		
$i\rightarrow j$	f_{ij}	ϵ_{ij} (meV)	$i\rightarrow j$	f_{ij}	ϵ_{ij} (meV)
$1\rightarrow 272$	0.35	94.3	$17\rightarrow 286$	0.022	85.75
$\mathbf{0\rightarrow 275}$	0.31	95.9			
$0\rightarrow \mathbf{391}$	0.28	119.6	$10\rightarrow \mathbf{415}$	0.012	115.85
$1\rightarrow 392$	0.27	120.6			
$0\rightarrow \mathbf{6}$	0.16	9.3	$28\rightarrow \mathbf{44}$	0.005	6.0

Table I shows the most important transitions at 4 and 300 K that contribute to each absorption spectrum. Note that now the system consists of hundreds to thousands of states, numbered (i,j) with increasing eigenenergy (as opposed to the simple subband numbering, $n=1\ldots 4$). We find that at low temperatures the spectrum is dominated by a *few* impurity transitions with *large* oscillator strength, whereas at room temperature it consists of hundreds (we only show one for each peak) of transitions between extended states with much *weaker* oscillator strength.[24] The wave functions of the ground and final states corresponding to the three strongest transitions at $T=4$ K, integrated over the z coordinate, are plotted in Fig. 3. The ground state and all final states are clearly localized.

The same analysis can be made for the strongest transitions at 300 K. As an example we plotted the wave functions of the final states $j=44$, and $j=415$ in Fig. 4, marking the final states of the $1\rightarrow 2$ and $1\rightarrow 4$ transitions, respectively. Since initial and final states have almost the same shape (integrated over the z coordinate), we omit here a detailed analysis for all contributing states. However, from Table I and Fig. 4 we see that at high temperatures the spectrum is

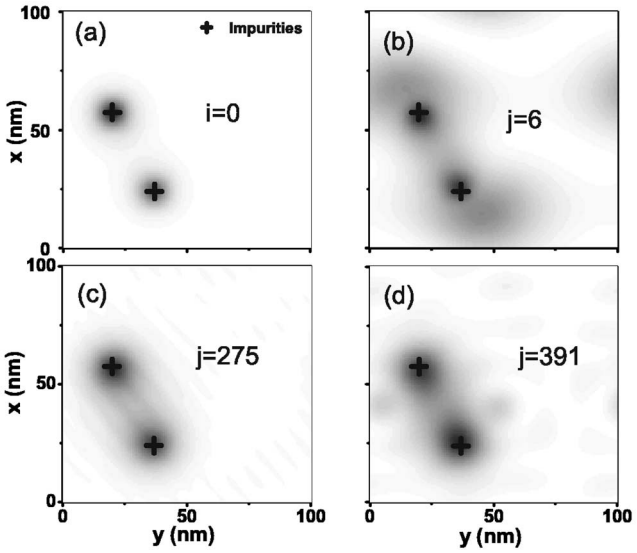

FIG. 3. Wave functions of the initial (a) and final states (b)–(d) that contribute the spectrum of the double QW at $T=4$ K.

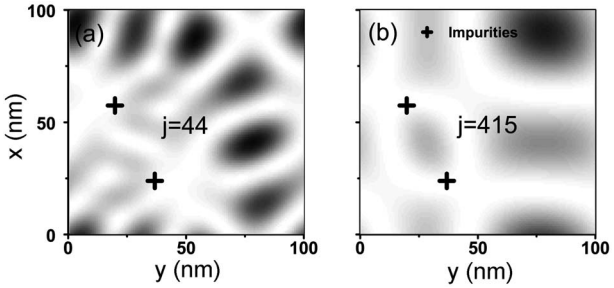

FIG. 4. Final states of the most important transitions contributing to the absorption spectrum of the double QW at $T=300$ K.

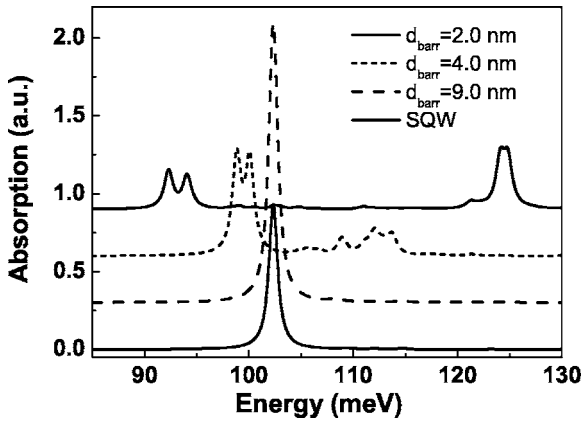

FIG. 5. Absorption spectra for the double QW with different barrier thicknesses and of a single QW for comparison at $T=4$ K. The spectra a vertically shifted for clarity.

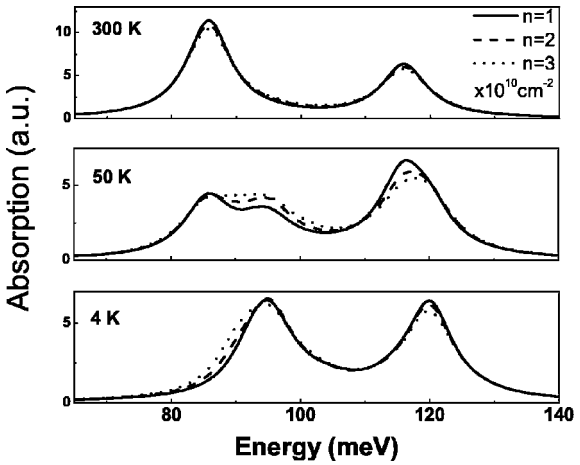

FIG. 6. Calculated normalized absorption of a double quantum well for different electron densities and temperatures.

dominated by many transitions between extended states.

Barrier thickness dependence. Now we want to discuss the influence of the barrier thickness that separates the two wells. Therefore we have calculated the low-temperature absorption spectra using a very—unrealistically—small broadening parameter ($\Gamma=0.5$ meV) to follow exactly its evolution from a single quantum well behavior to the one of a typical double QW with fixed well thicknesses of 9.0 nm. The results are shown in Fig. 5. We start with the comparison of a single QW spectrum to the double QW spectrum with a barrier thickness of 9.0 nm. Since the barrier is wide, the wells act independently of each other leaving the line position unchanged, but doubling the strength, since we have two impurities in the double QW and only one in the single QW. In the case of very strong coupling ($d_{\mathrm{barr}}=2$ nm) we observe two peaks at 94 and 124 meV, respectively, each of which is split again by a very small amount. Whereas the two large features correspond to the $1s$-$3d_0$ and $1s$-$4f_0$ transitions, the small splitting is probably due to a slightly different impurity configuration in the two QWs, and only visible due to the unrealistically high resolution. At intermediate coupling-barrier thickness ($d_{\mathrm{barr}}=4$ nm) the low-energy doublet at ≈ 99 meV is already well established, whereas the high-energy transitions are not clearly developed. This can most likely be attributed to the fact that for this barrier thickness the z-coupling strength (as measured by the splitting of the corresponding $n=3,4$ subbands) is of the same order as the Coulomb binding energy ($\mathrm{Ry}^* \approx 10$ meV). I.e., when the coupling strength is larger than one Ry^*, both subbands acquire their own impurity state, and for the opposite case of weak coupling there is only one impurity state below the exited subband manifold. In the intermediate range, all states (subband and impurity) are heavily mixed, defying a clear classification.

Doping concentration dependence. Also interesting is the effect of higher doping concentration, which we increased up to 3×10^{10} cm^{-2}. The integral absorption is proportional to the electron density, so we plotted the absorption behavior for doping densities of 1, 2, 3×10^{10} cm^{-2} normalized to 1 $\times10^{10}$ cm^{-2} in Fig. 6 for three different temperatures. Since impurity states play a role mostly at low temperatures, we would expect the strongest differences in this regime. In fact, this is what we observe in Fig. 6. At a temperature of 4 K, the absorption peak at 95 meV obtains an additional shoulder on the low-energy side, becoming stronger with increasing density. Obviously, the ground states of the additional impurity transitions are slightly higher in energy than that of a single impurity (i.e., more weakly bound), leading to a broader absorption line. At 50 K, however, this effect seems to be more pronounced. The $1s$-$3d_0$ transition becomes enhanced and broader with increasing doping density, since it now consists of several impurity transitions, leading to inhomogeneous broadening. Interestingly, the $1s$-$4f_0$ transition gets weaker at the same time, while the regular $2\rightarrow3$ transition remains unchanged. At high temperature, where transitions between impurity states become less important compared to the regular intersubband transitions, no significant changes in the absorption spectrum can be determined, which is in agreement with our previous expectations. So with increased doping we find that the impurity-related peaks in the spectrum become broader, and that the $1s$-$3d_0$ transition gets stronger compared to the intersubband transitions. Since we are limited to the low doping regime we cannot explore this phenomenon further, but it will be an interesting aspect once electron-electron interaction can be included in our model.

Impurity location dependence. Up to this point we were distributing the impurities in each QW randomly. While this method reflects the experimental case most realistically, we also want to show what happens if we place the single dopant atoms in each quantum well at different distances from each other in the (x,y) plane. This is not feasible with current experimental technologies, but since real samples will exhibit a random distribution of impurity separations, it is useful to understand the separation effects. Note the absolute position inside the well is irrelevant due to the periodic boundary conditions, which also limits the maximum separation. We calculated the absorption coefficient at a temperature of 4 K for different distances (0.01…70 nm) of the impurities in the (x,y) plane. The carrier density was set to 1 $\times10^{10}$ cm^{-2}, so that we have again one impurity per QW. The results of this calculation are shown in Fig. 7.

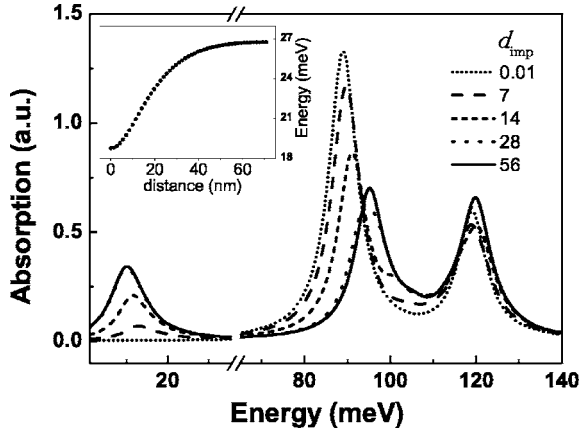

FIG. 7. Calculated absorption of a double quantum well for different lateral distances of the donors in each well at an electron temperature of 4 K. The inset shows the energy level of the ground state for different distances.

At a distance of more than 30 nm, we see the regular absorption spectrum deriving from impurity transitions in each well with three absorption peaks (at 10, 95, and 120 meV), just like before in Fig. 2. Once we reduce the distance in the (x,y) plane (note that both impurities are always separated in the z direction by 11.5 nm), we see drastic changes of the absorption behavior. While the spectral position of the peak at 120 meV does not change, both other peaks get shifted. Amazingly, the peak at 10 meV not only broadens and blueshifts, but also completely vanishes at very small distances. Apparently this transition becomes symmetry forbidden once the impurity levels start to couple in the z direction. We also observe major changes of the $1s$-$3d_0$ transition, namely a large redshift of $\approx$10 meV and a strong increase by a factor of 2. Thus, in the same way that the doublets in a double QW are obtained by moving two QWs closer together, now the impurity levels are split. To clarify this we plotted the energetic level of the ground state for various distances in the inset of Fig. 7. We see that the ground state (e.g., $1s$) gets lowered in energy by $\approx$8 meV, indicating that the formerly independent $1s$ states of each impurity now are split into a doublet. Of course this effect not only acts on the ground states but for all impurity states and thus leads to these drastic changes of the absorption spectrum. However, due to the complexity we omit a detailed study of all states contributing to the spectra as was done above. But as already mentioned, although this calculation is not directly comparable to a real absorption experiment, it still shows the possibility of an additional effect that can lead to an enhanced broadening of some absorption peaks, if the donor density is high enough that some impurities have a similar (x,y) position.

V. INCREASING THE NUMBER OF WELLS

A. Quadruple quantum well

It is now most interesting to increase the number of coupled wells and track the evolution into a superlattice. In the following we will calculate the absorption spectrum of a quadruple quantum well (QQW) that will be compared to experimental data, leading to an almost perfect agreement. After this we will increase the number of wells further up to 20, which will serve as a superlattice, and compare their absorption spectra.

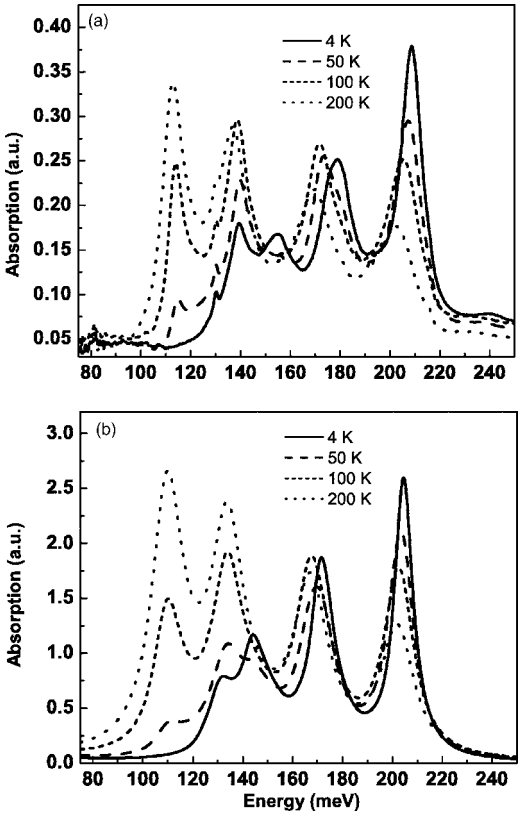

FIG. 8. Experimental (a) and calculated (b) absorption spectra of a quadruple quantum well shown for different temperatures.

So let us now turn to the case of a QQW. The QQW sample consists of 6.8-nm-wide GaAs wells separated by 2.5-nm-thin $Al_{0.32}Ga_{0.68}As$ barriers. This structure is repeated 120 times and separated by an undoped 20-nm-thick $Al_{0.32}Ga_{0.68}As$ layer. The average doping density over the four QWs with coupling barriers was 3×10^{16} cm^{-3}, resulting in a sheet density per QW of 2.6×10^{10} cm^{-2}. The sample was polished with 45° facets and the absorption was measured in a multiple reflection geometry by dividing the p-polarized spectra (where we have a light component parallel to the growth axis z) by the s-polarized one using a Fourier transform spectrometer. By placing the sample onto a cold finger liquid-He flow cryostat the absorption was measured at different temperatures. The experimental data are shown in Fig. 8(a).

At all temperatures, we observe four prominent peaks in the spectrum, however, their spectral position and strength drastically changes for different temperatures. At T=200 K, starting on the low-energy side, they can be attributed to the $4\rightarrow5$, $3\rightarrow6$, $2\rightarrow7$, and $1\rightarrow8$ transitions in the structure. At T=4 K, as for double QW, we can assign all peaks to transitions between localized states, namely impurity states.

This can be proven by a direct comparison to calculated absorption spectra for different temperatures, using the same

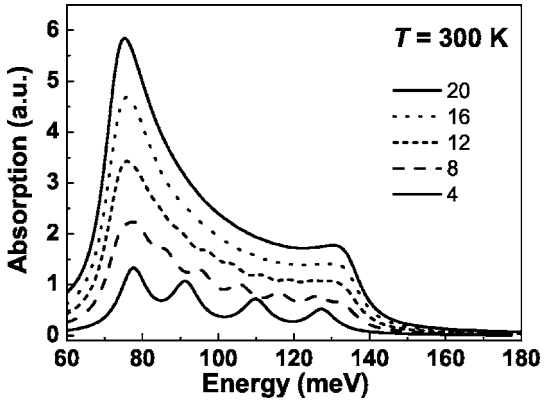

FIG. 9. Calculated absorption spectra at $T=300$ K for different numbers of quantum wells.

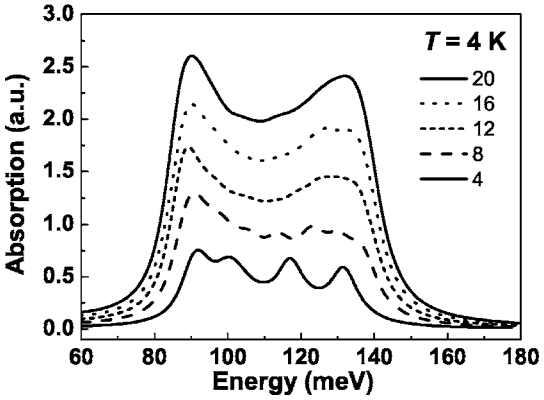

FIG. 10. Calculated absorption spectra at $T=4$ K for different numbers of quantum wells.

structure parameters as for the grown sample. This is shown in Fig. 8(b). To account for the different linewidths with varying the temperature, we adjusted the broadening parameter Γ from 4 meV at 4 K to 6 meV at 200 K. By comparing the experimental and theoretical results we observe excellent agreement in the peak positions and strengths, clearly demonstrating the validity of our model.

B. Towards the superlattice

Now we increase the number of wells further and follow the system's evolution into a superlattice. Therefore we use the same parameters as for the double quantum well calculations ($d_{\text{well}}=9.0$ nm, $d_{\text{barr}}=2.5$ nm) and a doping density of 1×10^{10} cm^{-2}, so that we have one impurity per QW. Let us first analyze the change of the absorption at $T=300$ K with increasing number of wells from 4 to 20. The results are shown in Fig. 9. For four wells, we observe a similar absorption shape as for the QQW above, having the strongest absorption at the $4\rightarrow5$ transition. By increasing the number of wells, this behavior remains and at 20 periods we see a smooth absorption spectrum. This reveals the typical absorption spectrum of a superlattice,[12] reflecting the van Hove singularities in the joint density of states at the edge of the mini-Brillouin zone ($k_z=\pi/d$) and at its center ($k_z=0$), respectively [see Fig. 1(c)]. The integrated absorption strength is proportional to the number of quantum wells.

We performed the same calculations for $T=4$ K, shown in Fig. 10. With only four periods, we see four clearly separated peaks that all derive from transitions between localized states, as mentioned above. Increasing the number of periods, the individual peaks merge into a broad spectrum that contains two pronounced maxima at 90 and 135 meV, respectively. The low-energy maximum is sharper due to the higher density of transitions, while the high-energy maximum becomes discernible only for more than ten periods. By increasing the number of periods, the formerly separated impurity states in each quantum well start to form impurity bands, that are attached to each miniband. Note, however, that this results from coupling in the z direction and not through wave-function overlap in the (x,y)-plane, the latter corresponding to the common notion of impurity bands.[25] As for single impurity states, they are slightly lower in energy than their corresponding minibands.[13] This is depicted in Fig. 1(c) as the grey shaded areas. Corresponding experimental spectra have been published in Ref. 13.

To prove this assumption, we have plotted the excited states that contribute to the absorption spectrum at 135 meV for low and high temperatures in Fig. 11. While the state 2310 in Fig. 11(a) is mainly localized around an impurity on the bottom left, there is no correlation between wave function and impurity location for state 2485 in Fig. 11(b). This clearly demonstrates that also for superlattices at low temperature we only have transitions between impurity states, in fact a broad absorption band. This modifies the previous assumption,[12] where only the lower energy peak (here at 90 meV) was ascribed to an impurity transition and the higher energy one to a miniband transition (at $k_z=0$).

In that previous work a superlattice (well width 7.5 nm, barrier width 2.5 nm) with doping concentration of 6×10^{16} cm^{-3} was studied. Magnetotransport experiments revealed a magnetic-field-induced metal-insulator transition in this sample, and far-infrared cyclotron and impurity resonance experiments proved that at $B>6$ T the Fermi energy at low temperature was in the impurity band.[26] Now we performed interminiband absorption experiment on this sample in a magnetic field along the z direction, in a 7-T split-coil magnet optical cryostat equipped with ZnSe windows. Assuming that the Fermi energy drops from the miniband into the impurity band at some magnetic field below 6 T one

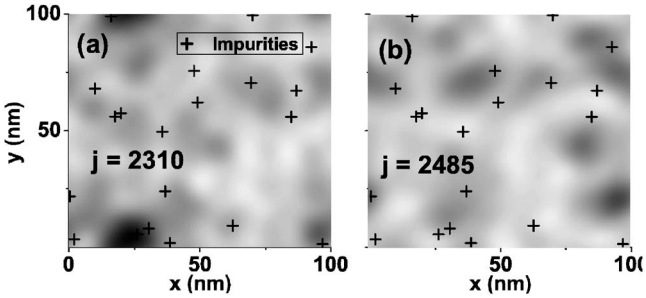

FIG. 11. Wave functions of the final states contributing to a transition at 135 meV at 4 K (a) and to a transition at 132 meV at $T=300$ K (b).

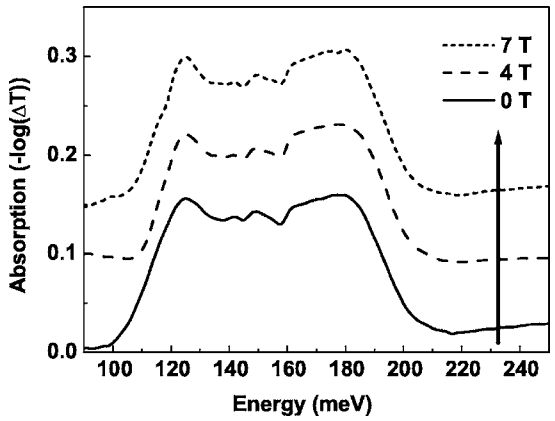

FIG. 12. Absorption spectra of a superlattice for magnetic fields $B=0$, 4, and 7 T, exhibiting no change with magnetic field. ΔT is the ratio of *p*- and *s*-polarized transmission, the curves are vertically shifted for clarity. The fine structure around 150 meV is probably due to some traces of organic solvents on the sample surface and not relevant here.

would expect that the high-energy peak—if ascribed to the $k_z=0$ interminiband transition—would disappear. However, the resulting spectra, displayed in Fig. 12, remain completely unchanged between $B=0$ and $B=7$ T. Their shape is similar to Fig. 10, only the energy scale is different due to the different sample parameters. This behavior *can only be explained assuming that the whole spectrum, including the high-energy peak, is due to an impurity transition*. This is a further striking prove of the existence of the above described impurity bands, attached to each miniband.

VI. SUMMARY AND OUTLOOK

We have presented a unified theory of confined impurity states in heterostructures, where the confining potential and the random impurity potential have been treated on the same footing. Calculation of infrared absorption spectra has provided insight into the interplay between impurity and subband states and facilitated the interpretation of experimental data. An extension of our theory to include a magnetic-field and electron-electron interaction may shed new light on the metal-insulator transition in confined semiconductor systems.

ACKNOWLEDGMENTS

We are grateful to J. J. Lee, N. Georgiev, and T. Dekorsy for help in the magnetoabsorption experiments. Sandia is a multiprogram laboratory operated by Sandia Corporation, a Lockheed-Martin Company, for the United States Department of Energy's National Nuclear Security Administration under Contract No.DE-AC04-94AL85000.

[1] K. Leo, *High-Field Transport in Semiconductor Superlattices* (Springer, New York, 2003).
[2] *Intersubband Transitions in Quantum Wells: Physics and Device Applications of Semiconductors and Semimetals*, Vols. 62 and 66 edited by H. C. Liu and F. Capasso (Academic, San Diego, 2000).
[3] G. Bastard, Phys. Rev. B **24**, 4714 (1981).
[4] C. Mailhiot, Y. C. Chang, and T. C. McGill, Phys. Rev. B **26**, 4449 (1982).
[5] R. Chen, J. P. Cheng, D. L. Lin, B. D. McCombe, and T. F. George, J. Phys.: Condens. Matter **7**, 3577 (1995).
[6] A. Bruno-Alfonso, G. Q Hai, F. M. Peeters, T. Yeo, S. R. Ryu, and B. D. McCombe, J. Phys.: Condens. Matter **13**, 9761 (2001).
[7] R. L. Greene and K. K. Bajaj, Phys. Rev. B **31**, 4006 (1985).
[8] In addition, the binding energy becomes z dependent, which, however, will not be discussed here further, since we assume all impurities to be located in the center of a quantum well.
[9] J. P. Cheng and B. D. McCombe, Phys. Rev. B **42**, 7626 (1990).
[10] T. A. Perry, R. Merlin, B. V. Shanabrook, and J. Comas, Phys. Rev. Lett. **54**, 2623 (1985).
[11] M. Carras, V. Berger, X. Marcadet, and B. Vinter, Phys. Rev. B **70**, 233310 (2004).
[12] M. Helm, W. Hilber, T. Fromherz, F. M. Peeters, K. Alavi, and R. N. Pathak, Phys. Rev. B **48**, 1601 (1993); M. Helm, Semicond. Sci. Technol. **10**, 557 (1995).
[13] D. Stehr, C. Metzner, M. Helm, T. Roch, and G. Strasser, Phys. Rev. Lett. **95**, 257401 (2005).
[14] S. T. Yen, Phys. Rev. B **68**, 165331 (2003).
[15] C. Priester, G. Allan, and M. Lannoo, Phys. Rev. B **29**, 3408 (1984).
[16] M. Helm, F. M. Peeters, F. DeRosa, E. Colas, J. P. Harbison, and L. T. Florez, Phys. Rev. B **43**, 13983 (1991).
[17] A. Ghazali and J. Serre, Phys. Rev. Lett. **48**, 886 (1982); J. Serre and A. Ghazali, Phys. Rev. B **28**, 4704 (1983).
[18] J. Serre, A. Ghazali, and A. Gold, Phys. Rev. B **39**, 8499 (1989).
[19] J. Kortus and J. Monecke, Phys. Rev. B **49**, 17216 (1994).
[20] M. Hofmann, M. Bockstedte, and O. Pankratov, Phys. Rev. B **64**, 245321 (2001).
[21] B. S. Monozon and P. Schmelcher, Phys. Rev. B **71**, 085302 (2005).
[22] C. Metzner, M. Hofmann, and G. H. Döhler, Phys. Rev. B **58**, 7188 (1998).
[23] R. N. Riemann, C. Metzner, and G. H. Döhler, Phys. Rev. B **65**, 115304 (2002).
[24] At low temperature Table I shows two almost identical transitions for each spectral position, deriving from the presence of two impurities in the complete system.
[25] S. Liu, K. Karrai, F. Dunmore, H. D. Drew, R. Wilson, and G. A. Thomas, Phys. Rev. B **48**, 11394 (1993).
[26] W. Hilber, M. Helm, F. M. Peeters, K. Alavi, and R. N. Pathak, Phys. Rev. B **53**, 6919 (1996).